J Mater Sci (2008) 43:4534–4540
DOI 10.1007/s10853-008-2642-x

Studies on ac response of zinc oxide pellets

P. P. Sahay · S. Tewari · R. K. Nath · S. Jha · M. Shamsuddin

Received: 10 December 2007 / Accepted: 8 April 2008 / Published online: 29 April 2008

Abstract The ac responses of the ZnO pellets have been studied by ac measurements (impedance, capacitance and phase angle) over the temperature range 300–435 K. The ac conductivity of the ZnO pellets is observed to be proportional to ω^s, where ω is the angular frequency and the exponent s is a temperature- and frequency-dependent parameter. Based on the existing theories of ac conduction, it has been concluded that for low frequency region (20 Hz–2 kHz), the dominant conduction mechanism in the ZnO pellets is multihopping at all temperatures, whereas for high frequency region (500 kHz–2 MHz), the small polaron tunneling model is the dominant mechanism in the pellets. Activation energies for ac conduction processes are estimated to be in the range of 0.028–0.277 eV which are found to vary with the frequency of the ac signal. These results are found to be consistent with the hopping model. The ac capacitance and the dielectric loss tangent are found to be dependent on both frequency and temperature. Such dependences have been explained taking into account the equivalent circuit model comprising a frequency-independent capacitive element in parallel with a temperature-dependent resistive element, both in series with a low value resistance. Impedance spectroscopy studies show single semicircular arcs in the complex impedance spectra at all temperatures in the range 300–435 K, with their centres lying below the real axis at a particular angle of depression indicating a multirelaxation behaviour in the pellets.

P. P. Sahay (✉) · S. Tewari · R. K. Nath
Department of Physics, National Institute of Technology, Silchar 788 010, India
e-mail: dr_ppsahay@rediffmail.com

Present Address:
P. P. Sahay
Department of Physics, Motilal Nehru National Institute of Technology, Allahabad 211 004, India

S. Jha · M. Shamsuddin
Department of Metallurgical Engineering, Banaras Hindu University, Varanasi 221 005, India

Introduction

Among transition metal oxide semiconductors, zinc oxide (ZnO) is a promising material for many device applications such as varistors, gas sensors, transparent electrodes, etc. [1–6]. Clarke [1] discussed ZnO materials for varistor applications. Viswanath et al. [2] have studied the preparation and characterization of nanocrystalline ZnO-based materials for device applications. Gas-sensing characteristics of porous ZnO and Pt/ZnO ceramics have been examined by Saito et al. [3]. Sprayed ZnO thin films for ethanol sensors have been investigated by Sahay et al. [4]. Gas-sensing properties of nano-ZnO prepared by arc plasma method have been studied by Dong et al. [6]. The various applications of ZnO are due to its significant physical and chemical properties. Being a non-ferrous electric compound and having large enough electromechanical coefficients, ZnO is a well-known piezoelectric material which has been used as a transducer for surface acoustic wave (SAW) devices [7]. This material has been investigated in the form of single crystals [8], sintered pellets [9], thick films [10], thin films [11] and heterojunctions [12]. Jones et al. [8] have studied the effect of the physical form of the oxide on the conductivity changes produced by CH_4, CO and H_2O on ZnO. Hydrothermal synthesis of highly crystalline ZnO nanoparticles for LPG and EtOH sensors has been investigated by Baruwati et al.

[9]. Arshak and Gaiden [10] have developed a novel gas sensor based on zinc oxide thick films [10]. Cheng et al. [11] have studied the preparation, characterization and gas-sensing property of ZnO nanoparticulate thin film. Modified heterojunction based on zinc oxide thin film for hydrogen gas-sensor application has been examined by Basu and Dutta [12].

Though studies on dc conductivity in ZnO material have received considerable attention of researchers, there have been only a few studies on their ac transport properties [13–15]. AC measurements are important means for studying the dynamic properties (conductance, capacitance and dielectric loss tangent) of the semiconducting and dielectric materials. They provide information about the interior of the materials in the region of relatively low conductivity. This measurement also helps to distinguish between localized and free band conduction. In the case of localized conduction, the ac conductivity increases with frequency, while in the free band conduction the conductivity decreases with frequency. Further, impedance spectroscopy is a well-known and powerful technique for investigating polycrystalline materials where the contribution of various processes such as bulk conduction, grain boundary conduction and transport across electrode-sample interface can be resolved in the frequency domain [16–19]. This technique has the advantage over dc techniques of being able to separate the electrical response of different regions of a material, provided their electrical responses are within the measuring range of the instrumentation and the time constants of the various regions differ by more than about one decade.

In this paper we report a detailed study on the ac response of the ZnO pellets and analyse them in the light of the existing theories with a view of understanding the conduction mechanism involved.

Experimental details

The ZnO powder was prepared by the hydrolysis method by adding ammonia solution to the $ZnCl_2$ solution. The precipitate thus obtained was washed thoroughly with distilled water until the chlorides were removed from the precipitate. The resulting precipitate was dried at 100 °C for 20 h and calcined at 700 °C for 6 h in air. The resulting mass was then crushed into fine powder and pelletized at a pressure of ~13 MPa to form cylindrical pellets by means of die and punch. These pellets were sintered at around 850 °C for 12 h in air. Sintered pellets were then trimmed by polishing into discs of 13 mm diameter and 2–3 mm thickness. Structural analysis of the pellets was made using PANalytical X'Pert Pro X-ray Diffractometer with Cu Kα radiation ($\lambda = 1.5418$ Å) as X-ray source at 40 kV and 30 mA in the scanning angle (2θ) from 20° to 90°.

For ac measurements, the flat faces of the pellets were coated with a thin layer of high temperature silver paste for making good electrical contacts. The pellet was then mounted on a home-made two-probe assembly which was inserted coaxially inside a resistance-heated furnace. The temperature of the pellets was monitored using a chromel-alumel thermocouple with the help of a Motwane digital multimeter (Model: 454). The ac measurements (impedance, capacitance and phase angle) were carried out using a Solartron impedance analyser (Model: 1260) in the frequency range from 20 Hz to 2 MHz with an oscillation level of 100 mV and data taken at 5 points per decade. All these measurements were conducted at different temperatures between 300 and 435 K. Throughout the measurements, the pellet in the furnace was allowed to equilibrate at each temperature for more than 10 min.

Results and discussion

XRD studies

Figure 1 shows the XRD pattern of a typical ZnO pellet. The observed XRD pattern is found to match with the ICDD Reference Pattern: Zinc Oxide, 01-070-8072, using X'Pert HighScore software. It is observed from the XRD that the ZnO pellets possess hexagonal structure with lattice constant $a = b = 3.2465$ Å and $c = 5.2030$ Å. The pellets are found to exhibit a number of diffraction peaks associated with various reflection planes of the crystal. The average grain size (D) is determined from the predominant intensity (101) peak using the Debye–Scherrer formula [20]

$$D = k\lambda/\beta \cos\theta \quad (1)$$

where k is the shape factor, λ is the wavelength of the X-ray, θ is the Bragg's angle and β is the corrected FWHM for instrumental broadening. Grain size thus calculated is found to lie in the range of 100–110 nm.

AC conductivity

Figure 2 shows the frequency dependence of ac conductivity of a typical ZnO pellet at different fixed temperatures on a log–log scale. At low frequencies the ac conductivity is found to be weakly frequency dependent. It is clear that at all temperatures the conductivity increases with increasing frequency having different slopes over three frequency regions: (I) 20 Hz–2 kHz; (II) 2–500 kHz; (III) 500 kHz–2 MHz. For each frequency region, the conductivity follows the power law relation

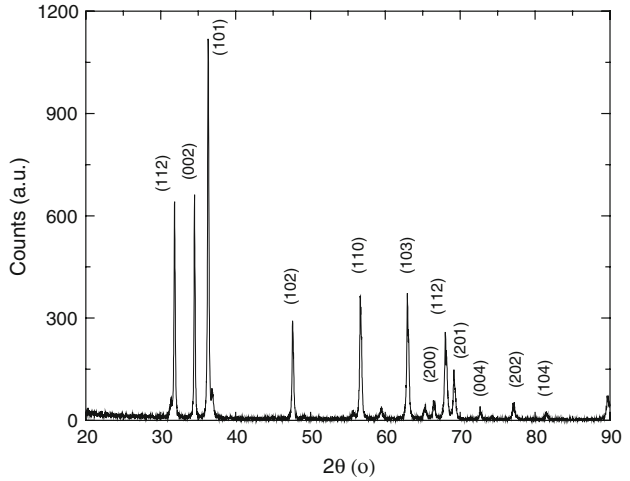

Fig. 1 XRD pattern of a typical ZnO pellet

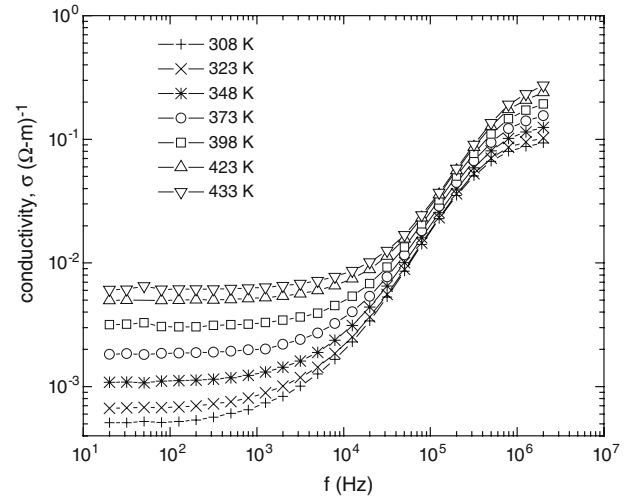

Fig. 2 Frequency dependence of ac conductivity of a typical ZnO pellet

$$\sigma = A\omega^s \tag{2}$$

where ω is the angular frequency, A is a constant and the exponent s is a frequency-dependent parameter and has values less than unity. Figure 3 shows the variation of s with temperature for three different frequency regions. For regions I and II, the exponent s is found to decrease with increasing temperature, while it increases with increasing temperature in region III.

Different theoretical explanations for the ac conduction in materials which contain both amorphous as well as crystalline phase have been developed to explain the frequency and temperature dependence of σ and s. According to hopping theory developed by Pollak and Geballe (PG), if hopping of charge carriers takes place between localized states with random distribution, the ac conductivity is directly proportional to ω^s where $0.5 < s < 1$ [21, 22]. It is

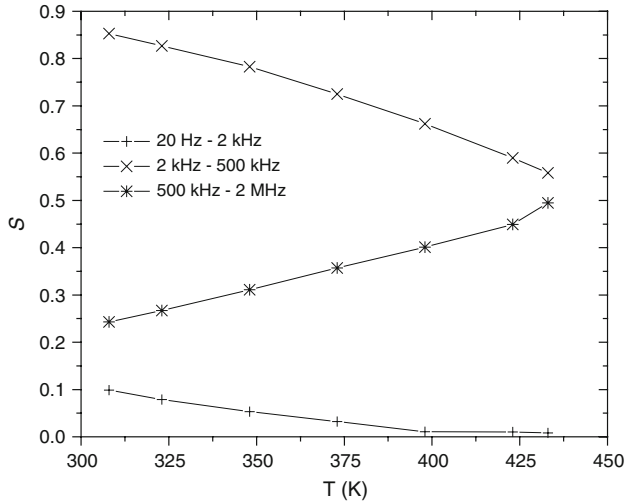

Fig. 3 Variation of the exponent s with temperature

known that the low values of s indicate multihopping process, while high values of s indicate single hopping process. This theory also predicts an increase in activation energy with decreasing frequency at higher temperatures. Further, Jonscher [23] showed that for hopping systems, it was possible to generate a range of power law relations with exponent s ranging from zero (corresponding to dc conductivity) to unity. He also found that s decreased with temperature and was frequency dependent. According to small polaron quantum mechanical tunneling model, the exponent s is an increasing function of temperature [24]. Based on these models, the present investigation leads to the following inferences.

(i) For frequency region I (20 Hz–2 kHz), the dominant conduction mechanism in the ZnO pellets is multihopping at all temperatures.
(ii) For region II (2–500 kHz), the conduction mechanism is multihopping at temperatures up to 348 K, while it is single hopping at temperatures beyond 348 K.
(iii) For region III (500 kHz–2 MHz), the small polaron tunneling model is the dominant conduction mechanism in the pellets which contributes to the ac conduction behaviour.

Figure 4 shows the variation of ac conductivity with inverse absolute temperature at six different frequencies. It is observed that the conductivity increases with increasing temperature at all frequencies. This may be due to thermally activated hopping of charge carrier between different localized states. Also, the pellets exhibit two activation energies at different temperature regions. The activation energy ΔE listed in Table 1 is calculated using the relation

$$\sigma = \sigma_0 \exp(-\Delta E/kT) \tag{3}$$

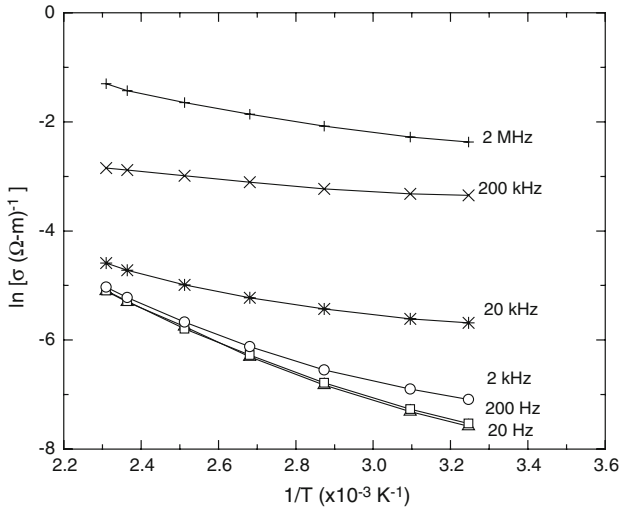

Fig. 4 Variation of ac conductivity with inverse absolute temperature

Table 1 Variation of activation energy with frequency

Frequency (Hz)	Activation energy (ΔE) in (eV)	
	Temperature region (308–348 K)	Temperature region (348–433 K)
20	0.175	0.277
2×10^2	0.173	0.274
2×10^3	0.126	0.252
2×10^4	0.060	0.146
2×10^5	0.028	0.061
2×10^6	0.068	0.127

where the symbols have their usual meanings. The observed behaviour of these activation energies with frequency is consistent with the models mentioned above, and could be associated with the energy required for charge carriers to be released from a set of shallow traps in the ZnO pellets.

AC capacitance

Figure 5 shows the variation of ac capacitance of the pellet with frequency at different fixed temperatures. It is clear that at all temperatures, the capacitance initially decreases rapidly with increasing frequency and subsequently approaches the low temperature values at higher frequencies. At low frequencies, the capacitance is strongly temperature dependent, while at high frequencies, the temperature dependence is found to be weak. These results are also shown in Fig. 6 where the capacitance is plotted as a function of temperature at various frequencies. This figure also represents that the capacitance is strongly frequency dependent at higher temperatures and lower frequencies.

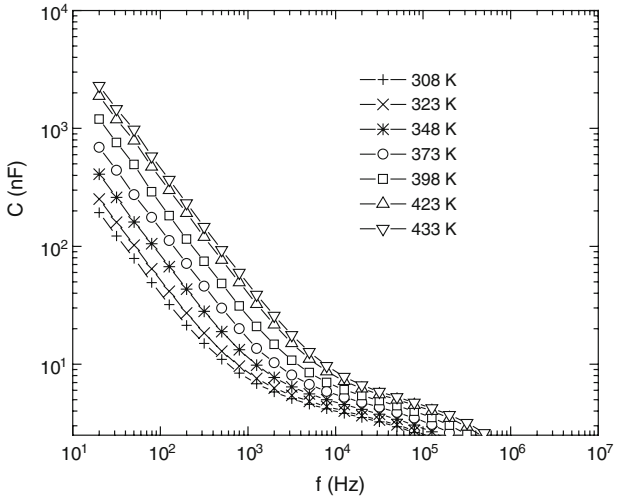

Fig. 5 Frequency dependence of ac capacitance

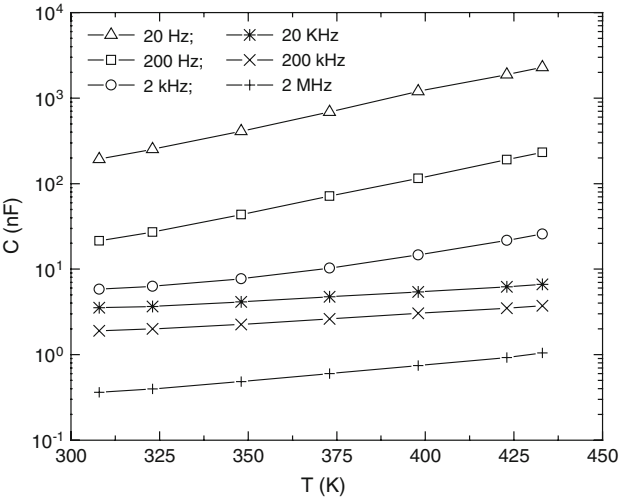

Fig. 6 Temperature dependence of ac capacitance

The observed variation of capacitance with frequency and temperature can be explained in accordance with the equivalent circuit model shown in Fig. 7, similar to that proposed by Goswami and Goswami [25]. The equivalent circuit comprises a frequency-independent capacitive element C_p in parallel with a temperature-dependent resistive element R_p, both in series with a low value resistance R_s. The measured series capacitance of such a circuit is given by

$$C = C_p + 1/(\omega^2 R_p^2 C_p^2) \quad (4)$$

The resistive element R_p is assumed to vary with temperature according to the relation

$$R_p = R_0 \exp(\Delta E/kT) \quad (5)$$

where R_0 is a constant and ΔE is the activation energy.

Equation 4 predicts that the measured capacitance C should decrease with increasing frequency at all temperatures.

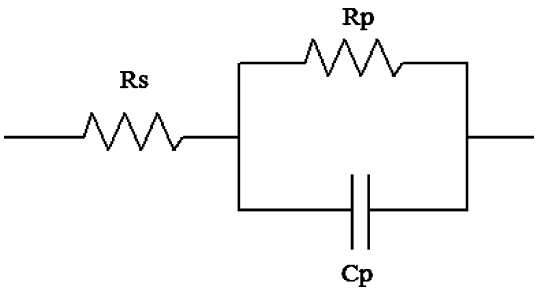

Fig. 7 Equivalent circuit model

Also, for any given frequency, the capacitance will increase with increasing temperature because of the decreasing value of R_p in accordance with Eq. 5. These are found to be consistent with our experimental observations. Similar results have been observed in several organic semiconductors such as thin films of cobalt phthalocyanine, CoPc, [26], zinc phthalocyanine, ZnPc, [27], metal-free phthalocyanine, H_2Pc, [28], etc. In addition, same behaviour has been observed in inorganic materials like Cd_3As_2 and CdTe thin films [29, 30]. Gould and Din [29] have found a wide dispersion in the capacitance values at lower frequencies in Cd_3As_2 thin film sandwich structure; however, at temperatures less than 300 K, the capacitance decreases slightly with frequency but increases monotonically with temperatures greater than 300 K at all frequencies in the range of 500 Hz–20 kHz used. Ismail and Gould [30] have examined the ac conductivity and capacitance measurements on thermally evaporated CdTe thin films. In this case, measurements of capacitance C as a function of frequency and temperature showed a decrease in C with increasing frequency tending towards a constant value for all temperatures. C also increased with increasing temperature, with the most significant increase occurring at low frequencies.

Dielectric loss tangent (tan δ)

Variations of tan δ with frequency and temperature are shown in Figs. 8 and 9. Considering the equivalent circuit shown in Fig. 7, the loss tangent is given by

$$\tan\,\delta = ((1 + R_s/R_p)/(\omega C_p R_p)) + \omega C_p R_p \qquad (6)$$

In this equation, at low frequencies the term ω^{-1} is dominant and at high frequencies the term ω is dominant. Therefore, this equation predicts a decrease in tan δ at low frequencies followed by a loss minimum and again an increase in tan δ at high frequencies. In the present investigation, the observed frequency and temperature dependence of tan δ is quite consistent with those predicted by the equivalent circuit model, described above. Abu-Hilal et al. [31] have observed a minimum in tan δ versus f curves

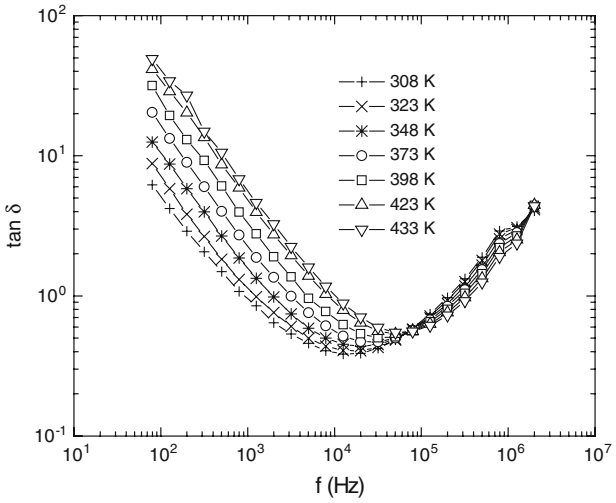

Fig. 8 Frequency dependence of dielectric loss

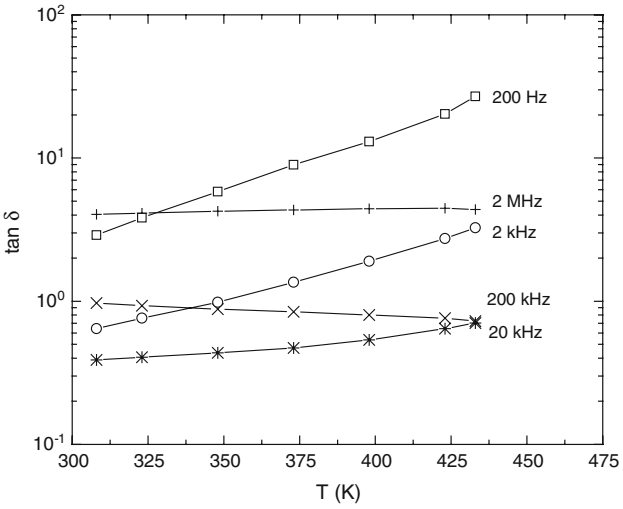

Fig. 9 Temperature dependence of dielectric loss

in ZnPc semiconducting thin films. Shihub and Gould [26] have reported decreasing values of tan δ with increasing frequency in CoPc thin films with no indication of a minimum, probably due to the limited frequency range of 100 Hz–20 kHz used. Choudhary and Bhunia [32] have shown a decrease in tan δ with increasing frequency tending towards a constant value, in case of $ACu_3Ti_4O_{12}$ (A = Ca, Sr and Ba).

Impedance spectroscopy

Figure 10 shows the Cole–Cole plots of Z' versus Z'' (where Z' and Z'' are the real and imaginary parts of the complex impedance, respectively) of the pellet at different temperatures over the frequency region from 20 Hz to 2 MHz. These plots are single semicircular arcs with their centres lying below the real axis at an angle θ. The finite

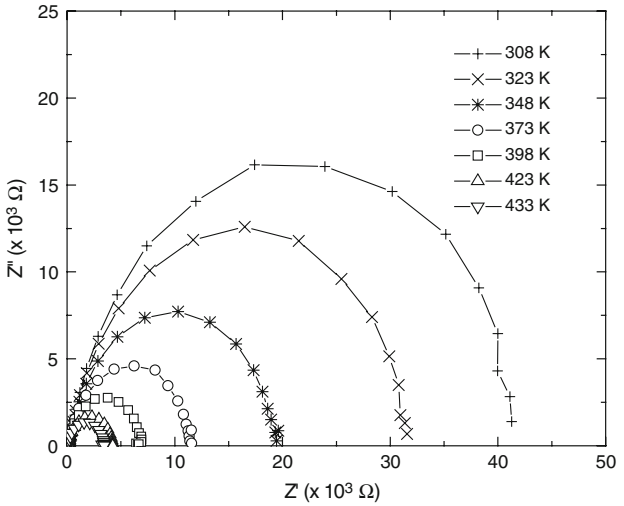

Fig. 10 Cole–Cole plots of imaginary impedance, Z'', versus real part, Z'

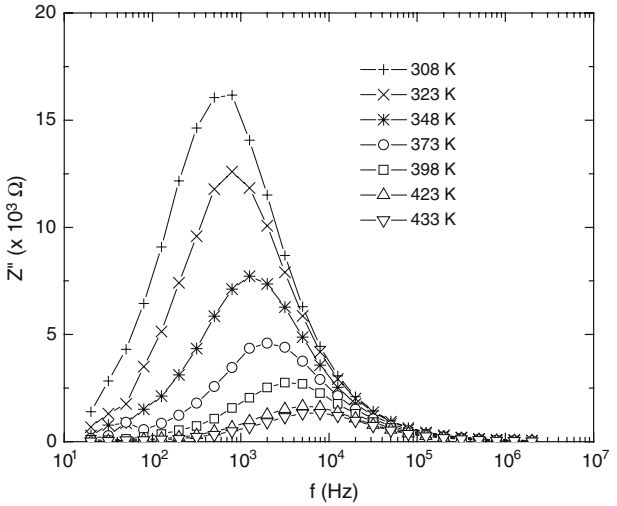

Fig. 11 Variation of Z'' with frequency

value of distribution parameter θ and a depressed arc are typical for a material with multirelaxation processes [33]. Also, the arcs have a non-zero intersection with the real axis in the high frequency region. Further, there occurs a reduction in the size of these plots with rise in temperature. Bose et al. [34] have studied the room temperature complex impedance spectra for nanocrystalline SnO_2 samples and observed the impedance spectra as depressed single semicircular arcs for different samples corresponding to their grain boundaries. Similar results have also been observed for the spray deposited films of ZnO [15] and the solution grown films of $CuInSe_2$ [35].

A single arc is an indicative of a single parallel RC element [17], as shown in Fig. 7. Here, the small resistance value R_s is attributed to the core of the ZnO grains, in accordance with the generally accepted view, while R_p and C_p are attributed to the grain boundary effect. Considering the equivalent circuit model, the values of Z' and Z'' are given by

$$Z' = R_s + R_p/(1 + \omega^2 C_p^2 R_p^2) \tag{7}$$

and

$$Z'' = -\omega C_p R_p^2/(1 + \omega^2 C_p^2 R_p^2) \tag{8}$$

These equations predict that the values of Z' and Z'' should decrease with increasing temperature as the values of R_p and R_s go on decreasing with rise in temperature in accordance with Eq. 4. This causes shrinking of the Cole–Cole plots with increase in temperature.

Figure 11 shows the spectra of Z'' versus frequency at different temperatures. These spectra are found to exhibit Debye peaks at different temperatures, and the peak maxima shifts to the high frequency side with increasing temperature. Similar results have also been reported by Dhananjay et al. in case of Mn-doped ZnO thin films [14].

The frequency ω_{max} at which Z'' is maximum is given by

$$\omega_{max} = 1/R_p C_p = 1/\tau \tag{9}$$

where τ is the relaxation time. As the value of R_p decreases with rise in temperature, ω_{max} should be an increasing function of temperature which is observed experimentally.

Summary and conclusions

Studies on ac response of the ZnO pellets have been carried out by ac measurements (impedance, capacitance and phase angle) over the temperature range (300–435 K). XRD studies on the pellets reveal that the material is of polycrystalline nature having hexagonal structure with lattice constant $a = b = 3.2465$ Å and $c = 5.2030$ Å. Grain size is found to lie in the range of 100–110 nm. Based on the existing theories of ac conduction, the dominant conduction mechanism in the ZnO pellets is found to be multihopping at all temperatures for low frequency region (20 Hz–2 kHz), while the small polaron tunneling model is the dominant mechanism in the pellets for high frequency region (500 kHz–2 MHz). Dependences of the ac capacitance and the dielectric loss tangent on the frequency and the temperature have been explained in accordance with the equivalent circuit model comprising a frequency-independent capacitive element in parallel with a temperature-dependent resistive element, both in series with a low value resistance. All the impedance spectra are found to have single semicircular arcs with non-zero intersection with the real axis in the high frequency region and also have their centres lying below the real axis at a particular angle of depression, indicating a multirelaxation

behaviour in the pellets. Thus, the present investigation gives an insight about the conduction mechanism involved in the sintered ZnO pellets.

Acknowledgements One of the authors (PPS) is grateful to Indian National Science Academy, New Delhi, for providing INSA Visiting Fellowship under which a part of the present investigation has been carried out at Department of Metallurgical Engineering, Banaras Hindu University, Varanasi, India.

References

1. Clarke DR (1999) J Am Ceram Soc 82:485
2. Viswanath RN, Ramasamy S, Ramamoorthy R, Jayavel P, Nagarajan T (1995) Nanostruct Mater 6:993. doi:10.1016/0965-9773(95)00229-4
3. Saito S, Miyayama M, Koumoto K, Yanagida H (1985) J Am Ceram Soc 68:40. doi:10.1111/j.1151-2916.1985.tb15248.x
4. Sahay PP, Tewari S, Jha S, Shamsuddin M (2005) J Mat Sci 40:4791. doi:10.1007/s10853-005-0519-9
5. Greuter F, Blatter G (1990) Semicond Sci Technol 5:111
6. Dong LF, Cui ZL, Zhang ZK (1997) Nanostruct Mater 8:815. doi:10.1016/S0965-9773(98)00005-1
7. Van De Pol FCM (1990) Ceram Bull 69:1959
8. Jones A, Jones TA, Mann B, Griffith JG (1984) Sens Actuators 5:75. doi:10.1016/0250-6874(84)87008-0
9. Baruwati B, Kumar DK, Manorama SV (2006) Sens Actuators B 119:676. doi:10.1016/j.snb.2006.01.028
10. Arshak K, Gaiden I (2005) Mater Sci Eng B 118:44. doi:10.1016/j.mseb.2004.12.061
11. Cheng XL, Zhao H, Huo LH, Gao S, Zhao JG (2004) Sens Actuators B 102:248. doi:10.1016/j.snb.2004.04.080
12. Basu S, Dutta A (1994) Sens Actuators B 22:83. doi:10.1016/0925-4005(94)87004-7
13. Ondo-Ndong R, Ferblantier G, Pascal-Delannoy F, Boyer A, Foucaran A (2003) Microelectron J 34:1087. doi:10.1016/S0026-2692(03)00198-8
14. Nagaraju DJ, Krupanidhi SB (2006) Mater Sci Eng B 133:70. doi:10.1016/j.mseb.2006.05.005
15. Sahay PP, Tewari S, Nath RK (2007) Cryst Res Technol 42:723. doi:10.1002/crat.200610895
16. Hong YW, Kim JH (2004) Ceram Int 30:1307. doi:10.1016/j.ceramint.2003.12.026
17. Andres-Verges M, West AR (1997) J Electroceramics 1:125
18. Jose J, Khadar MA (1999) Nanostruct Mater 11:1091. doi:10.1016/S0965-9773(99)00399-2
19. Abram EJ, Sinclair DC, West AR (2003) J Electroceramics 10:165
20. Klug HP, Alexander LE (1974) X-ray diffraction procedures for polycrystalline and amorphous materials. Wiley, New York
21. Pollak M, Geballe TH (1961) Phys Rev 122:1742. doi:10.1103/PhysRev.122.1742
22. Pollak M (1971) Philos Mag 23:519. doi:10.1080/14786437108216402
23. Jonscher AKJ (1972) Non-Cryst Solids. 810:293 doi:10.1016/0022-3093(72)90151-2
24. Meng LJ, Adritsck YM, Dos Santos MP (1994) Vacuum 45:19. doi:10.1016/0042-207X(94)90334-4
25. Goswami A, Goswami AP (1973) Thin Solid Films 16:175. doi:10.1016/0040-6090(73)90166-1
26. Shihub SI, Gould RD (1995) Thin Solid Films 254:187. doi:10.1016/0040-6090(94)06240-L
27. Saleh AM, Abu-Hilal AO, Gould RD (2003) Curr Appl Phys 3:345. doi:10.1016/S1567-1739(02)00243-2
28. Amar NM, Saleh AM, Gould RD (2003) Appl Phys A 76:77. doi:10.1007/s003390201306
29. Gould RD, Din M (1999) Superficies y Vacio 9:230
30. Ismail BB, Gould RD (1996) Proc SPIE 2780:46. doi:10.1117/12.238200
31. Abu-Hilal AO, Gould RD, Abu-Taha MI, Saleh AM (2007) Int J Mod Phys B 21:55. doi:10.1142/S021797920703587X
32. Choudhary RNP, Bhunia U (2002) J Mater Sci 37:5177. doi:10.1023/A:1021019412533
33. Macdonald JR, Johnson WB (2005). In: Barsoukov E, Macdonald JR (eds) Impedance spectroscopy: theory, experiment and applications. Wiley-Interscience, NJ
34. Chandra Bose A, Balaya P, Thangadurai P, Ramasamy S (2003) J Phys Chem Solids 64:659. doi:10.1016/S0022-3697(02)00368-2
35. Lal M, Batham PK, Goyal N (1995) Sol Energy Mater Solar Cells 36:111. doi:10.1016/0927-0248(94)00166-P